Ultra-Compacted Antenna-based Capsule Endoscope in the ISM Band

Marwah M. Hassooni[1], Jabir S. Aziz[2], Ashwaq Q. Hameed[3] and Hadeel Safa Hussein[1]
[1]Department of Electrical Engineering, College of Engineering, Al-Iraqia University, Baghdad, Iraq
[2]Al-Rafidain University, College, Baghdad-Iraq
[3]College of Electrical Engineering, University of Technology, Baghdad, Iraq

Corresponding author: Marwah M. Hassooni (e-mail: hassoonimarwa@gmail.com).

ABSTRACT This article presents a proposal for the miniature implantable antenna of a microstrip patch that covers ISM bands (2400–2483.5 MHz) for deep-tissue implantation with a volume of just 0.3 mm³. The proposed antenna is the smallest and lightest antenna manufactured for wireless capsule endoscopy. The antenna can be integrated with an imaging sensor, electronic components, and a battery. The proposed Microstrip Patch Antenna MPA shows a 483 MHz wider bandwidth at 2483.5 MHz; Beef muscles were used to validate the antenna's performance experimentally. The safety issues are assessed to examine the performance of the proposed antenna incorporated in an endoscopy capsule device by considering the specific absorption rate (SAR).

INDEX TERMS: Implanted devices, Microstrip Antenna, Miniaturization, Wireless Capsule Endoscope System.

I. INTRODUCTION

One of the most crucial considerations after antenna performance is the miniaturization and the biocompatibility of the implanted medical device within the body. Specific positions within the ingestible system are examined by wire endoscopy [1]. Ingestible and implantable medical devices support the diagnosis process in real-time images. To make an endoscopy lightweight and easy to handle, swallow, and not require anesthesia. All embedded components must be smaller to improve and enhance the quality of life by increasing the safety and effectiveness of emerging medical implantable antennas. Hence, the design of implantable and ingestible antennas for biomedical applications has attracted considerable attention and interest [2]. Although a miniature conformal antenna for ingestible capsule endoscopy in the (401-406 MHz) band is proposed by K.A. [3], the design is significant. S. Helmy proposed A specialized quadfilar or octafilar helical antenna (QFHA or OFHA) operating at a frequency of 2.4 GHz with circular polarization explicitly designed for wireless in-body capsule endoscopy applications [4], so the structure is complicated. In [5], Y. Alamgir presents a conformal antenna for multitasking, though the antenna is 57 mm³ in volume. In [6] proposes an implantable antenna for implantable biomedical devices in planar or conformal arrangements. However, the antenna is printed on the capsule's external wall, requiring another layer to be added to the capsule. K. Zhang et al. [7] present a conformal differentially-fed antenna for monitoring in-body core temperature. The simulated impedance bandwidth is 81.435 MHz. Although this antenna is simulated in different scenarios, it has a bulk volume of 30 mm³ and a relatively small bandwidth. In [8], an article introduces an inverted-F antenna explicitly designed for a capsule endoscope. The antenna functions in the 2.4 GHz band. It has a broad bandwidth of 151 MHz and an antenna gain of -3.13 dBi. In[9], a study presents a microstrip patch antenna designed to operate within the Medical Implantable Communication Service MICS frequency range. The antenna is constructed explicitly with dimensions of 20 mm in length and 30 mm in width. It operates at a frequency of 402.5 MHz with an omnidirectional radiation pattern. The reflection coefficient value was −15.07 dB, VSWR 1.428. In [10], the conformal capsule antenna has been designed specifically for use in ingestible wireless capsule endoscope (WCE) systems operating inside the Industrial, Scientific, and Medical (ISM) band, which spans from 2.4 to 2.48 GHz. A circularly polarized conformal wideband antenna is developed for a capsule endoscope system in the 915 MHz ISM band [11]. However, the helical and conformal implantable antenna structure increases the prototype's profile. Therefore, this work presents a new miniaturized microstrip capsule antenna. An ISM operation is considered in this study, i.e., data transmission at 2.4 GHz. The planar structure has been used in the designed antenna. The suggested antenna has a volume of 0.3 mm³ (1.5 × 1.9 × 0.12 mm); to our knowledge, it is the most miniature

microstrip implantable antenna modeled for applications of capsule endoscopy.

A. METHODOLOGY

In the present work, our attention is directed to a microstrip antenna for wireless capsule endoscopy operating within the industrial, scientific, and medical (ISM) bands (i.e., 2.4GHz). Wireless capsule endoscopy is implanted in deep tissue, displayed in Fig.1. This capsule houses essential components, including a battery, circuitry, and a Perfect Electric Conductor PEC which is encapsulated by a material made of Polycarbonate PC having a thickness of 0.3 mm, with $\varepsilon_r = 3$, and then implanted in a homogeneous tissue. Furthermore, the geometric dimensions of the endoscopy capsule were 23 mm ×9 mm. In the design of a basic rectangular microstrip antenna, the starting point is the specified information, which is calculated using the following formula [28], [12]:

$$L = \frac{c}{2 \times f\sqrt{\varepsilon_r}} \quad (1)$$

Where f is the resonant frequency, c speed of light, and ε_r is the dielectric constant of the substrate. Additional optimizations and iterative improvements have been made, which include the Defect Ground Technique (DGT) and a meandered line structure.

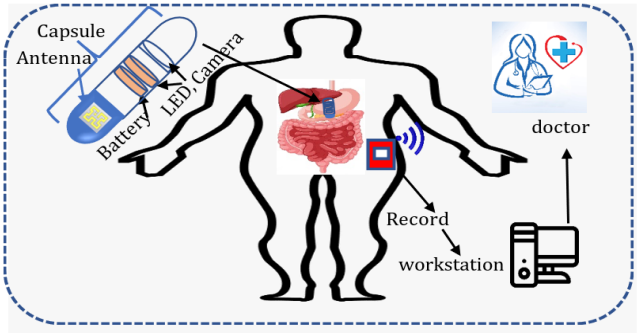

FIGURE 1. Capsule endoscopy system for imaging within the human body.

B. ANTENNA DESIGN

Geometric characteristics of the proposed implanted antenna with dimensions of 1.5mm×1.9 mm × 0.12 mm are displayed in Fig. 2. As depicted in Fig. 2(a) and (b), the patch with serpentine structure and slots within the base structure is fundamental to a considerable reduction in size, adjusting to the required operating frequency. The radiator of the designed microstrip antenna is printed on Rogers RO3010 of a thickness of 0.12 mm substrate dielectric constant (ε_r) = 10.2 and loss tangent (tanδ) = 0.0022, the high value of the dielectric constant an important technique used for miniaturization [13], The substrate material features a dual-layer copper cladding, where each copper layer has a thickness of 35 micrometer. Table I presents all the parameters of the proposed antenna. A coaxial feed of 50 Ω and a radius of 0.2 mm was utilized for the excitation of the antenna. The slotting technique has been used in the proposed antenna for optimized purposes in the ground plane to achieve optimum antenna performance and an impedance-matched resonance with the small structure in the relevant operating bands [14].

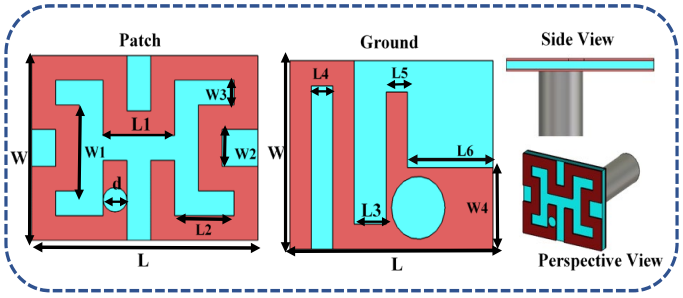

FIGURE 2. The proposed miniature antenna construction and dimensions are in mm.

TABLE I. The parameters of the proposed antenna

Variables	Values (mm)	Variables	Values (mm)
L	1.9	L5	0.2
W	1.5	L6	0.9
L1	0.6	W1	0.7
L2	0.5	W2, W3	0.3
L3	0.3	W4	0.7
L4	0.6	d	0.2

C. COMPUTATIONAL CONFIGURATION and MODELING

A finite-element method-based CST was used to design and analyze the suggested antenna. Firstly, a consistent muscle-mimicking material was simulated with dimensions of 80 × 80 × 60 mm^3 for an implanted antenna, as illustrated in Fig. 3. The relative permittivity of muscle tissue is 52.792. Its electrical conductivity is 1.705 Siemens per meter [15] at the resonant frequency of 2.450 GHz. The dielectric parameters of human tissues are presented well by Gabriel et al. Wireless signals attenuate in biological tissues, especially at commonly used frequencies like 2.4 GHz [16],[17]. An iterative improvement is implemented upon the design within a homogeneous phantom in a single-layer tissue.

The presented antenna is integrated into the dummy system, including a battery, PEC, and LED. A four-stage design optimization process was applied to assess the functionality of the suggested antenna throughout the desired frequency ranges, as depicted in Fig. 4. A basic rectangular radiator antenna was adopted. Then, a proposed MPA was designed. Additionally, the meandered line-patch shape and the use of open-ended slot structures in the ground layer of a traditional rectangular-patch antenna design reduced the antenna's physical footprint and enhanced overall antenna functionality. Fig. 4 illustrates the four major phases of the

design optimization method for the implanted antenna, each marked by iterative improvements. In the initial design phase (step 1), the ground layer remains unmodified, while the radiator shape suffers modifications, and a coaxial probe feed is used to excite the antenna. In this structure, the antenna resonates at a frequency proximate to 3.8 GHz. The next phase of the process involves an essential reconfiguration implemented by trimming the top left of the ground plane, which is one of the most admired techniques for antenna miniaturization.

Consequently, the antenna's operating frequency has been adjusted to 3.1 GHz. In Step 3, a rectangular slot is integrated into the ground layer. This modification enables the antenna to operate close to the required band frequencies, making it more versatile. Additionally, at this point, the antenna resonates at a frequency of 3 GHz. Finally, an additional rectangle slot inserted in the ground layer makes the proposed ultra-small antenna resonant at ISM-band 2.48GHz. Fig. 5 illustrates the S_{11} comparison between these four transit steps of variation in the suggested antenna.

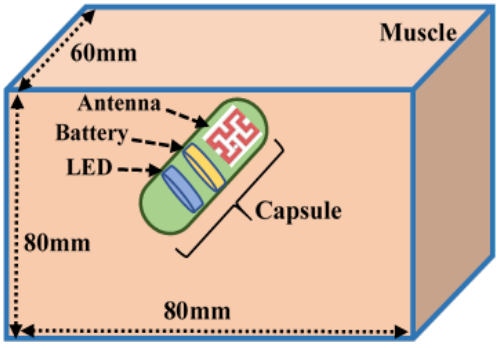

FIGURE 3. The muscle phantom model was used in the proposed antenna simulation.

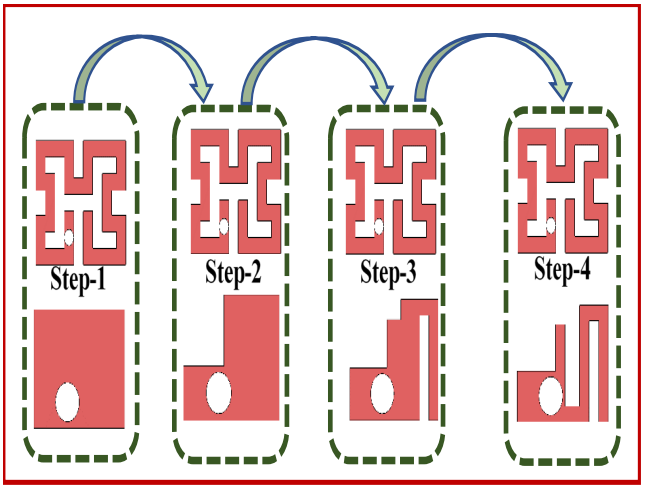

FIGURE 4. Various stages are involved in designing a small antenna.

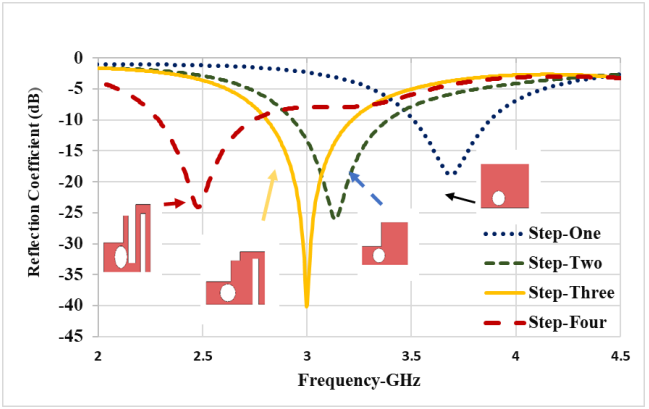

FIGURE 5. Various stages are involved in designing a small antenna.

II. PARAMETRIC STUDY OF MODEL

A. OPEN-END SLOTS WIDTH L3, L6

Fig. 6 depicts the effect of changing the width of the open-ended slots (L3), spanning from 0.1 to 0.4 mm, and the reflection coefficient S_{11} of the antenna. Increasing the width of the open-end slot (L3) causes the resonance frequency to shift towards a lower frequency. This shifting can be attributed to the open-ended slot being modeled as a resonant circuit, where the slot behaves like a capacitor and inductor in parallel. The specific dimensions of the slot, including its width (L3), influence this resonant circuit's effective capacitance and inductance.

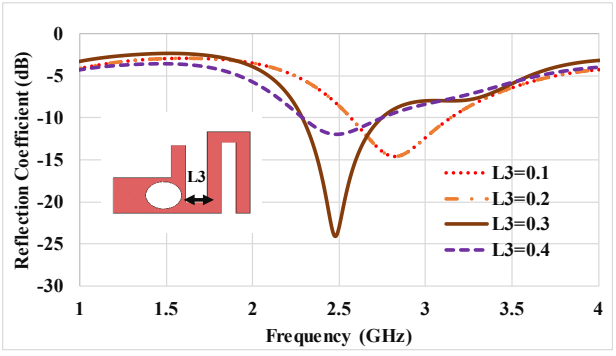

FIGURE 6. Impact on the S_{11} characteristics of the microstrip patch antenna owing to the L3 slot width variation.

Additionally, including other slots in the ground plan has enabled miniaturization of the antenna size and added extra capacitance. As the value of L6 increases from 0.2 mm to 0.9 mm, the resonant frequency of the antenna, indicated by the S_{11} curve, shifts towards lower frequencies. Shifting is evident from the left shift of the S_{11} curve as L6 increases and makes it operate at lower frequencies than the initial one, owing to the additional capacitance increasing the total capacitance of the suggested antenna [14], as illustrated in Fig.7.

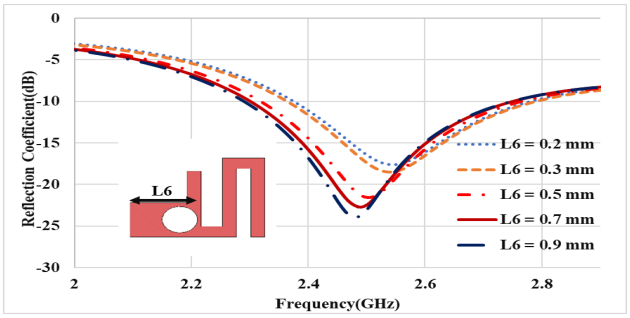

FIGURE 7. Impact on the S_{11} characteristics of the microstrip patch antenna owing to the L6 slot width variation.

B. OPEN-END SLOT LENGTH W5

The variations considerably influence the reflection coefficient S_{11} behavior of the suggested implantable microstrip antenna in the length W5 of the slot within the range of 0.6 mm to 1.3 mm, as depicted in Fig. 8.

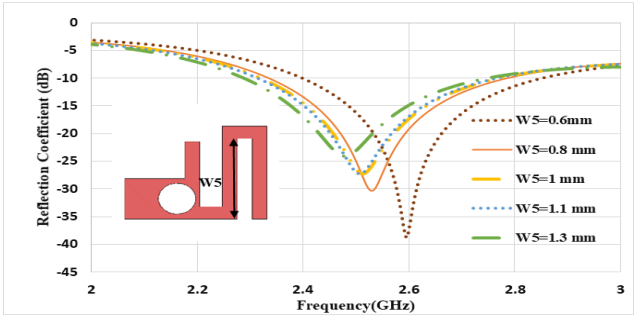

FIGURE 8. Influence of slot length W5 variation on the reflection coefficient

As the slot length increases from 0.6 mm to 1.3 mm, the resonance frequency of the antenna shifts towards lower frequencies. It is evident from the primary resonance peak that it moves from higher to lower frequencies as the slot length increases. The impedance bandwidth of the antenna, which is the frequency range over which the reflection coefficient (S_{11}) is below a certain threshold (typically -10 dB), increases as the slot length increases and can be seen from the broader frequency range over which the S_{11} values remain below the -10 dB level for more considerable slot lengths-showing the importance of the appropriate value of W5 in adjusting the proposed antenna.

C. FEEDING POSITION

Selecting the optimal position that provides the required performance features, such as operating frequency, bandwidth, and impedance matching, is essential in designing and optimizing implantable antennas. The notable differences in the reflection coefficient curves for the various feeding locations suggest that the position of the coaxial cable connection to the antenna significantly impacts the reflection coefficient, where the ground plane is not exposed to any modification, as depicted in Fig. 9. Consequently, it is the overall performance and operating frequencies. Positions 1 and 2 give resonant frequencies around 4 GHz.

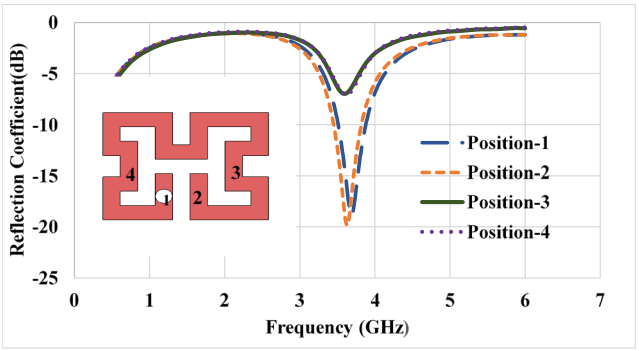

FIGURE 9. Effect of the feed point positions on the reflection of the proposed antenna.

III. ANALYSIS OF MODEL INTEGRITY

Reflection coefficient curves provide information about how well the implanted antenna functions in different implementation scenarios, as shown in Fig. 10. The findings observed in the stomach and colon regions suggest the antenna can achieve good impedance matching and resonance in these areas, which could enable efficient signal transmission for targeted applications. The broader, deeper dip in the muscle tissue curve indicates the antenna improved its matching in this environment. Still, the overall results demonstrate the versatility of the design and its potential for successful integration within the human body. The slight shifting in frequencies owing to the diversity of electrical properties of human tissues is represented as the dielectric constant and conductivity [6] listed in Table II. Owing to this reason, the ε_r and σ values of the tissues around the antenna (muscle) increased from 60% to 120% of their initial levels at a frequency of 2.45 GHz. The relative permittivity (ε_r) of the tissue surrounding it ranged from 31 to 64, whereas the conductivity (σ) of the muscle varied between 1 and 2 [18].

TABLE II. Electrical properties at the frequency (2.48GHz) of different tissue types

TISSUE TYPES	MUSCLE[15]	COLON	STOMACH
PERMITTIVITY	52.8	53.879	65
CONDUCTIVITY (S/M)	1.7	2.00	1.19

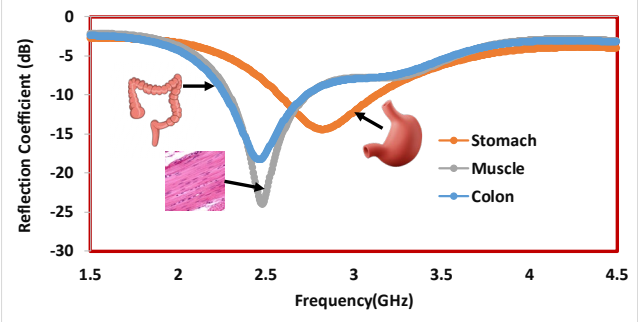

FIGURE 10. Reflection coefficient of the proposed antenna in different scenarios.

A. CURRENT DISTRIBUTIONS AND RADIATION PATTERNS

Fig. 11 depicts the current distribution of the suggested antenna. Within the 2.48 GHz spectrum operating frequency, a sensible current concentration is observed around the antenna's feed point. Furthermore, the current density is observed along the meandered path from the excitation point along this line on both the antenna's left and right parts. The current flow appears to be concentrated along the edges and corners of the microstrip, a common characteristic of microstrip antenna designs. Additionally, an essential current density concentration can be observed around the feed points on the opposing side of the ground layer, as shown in Fig. 11(b).

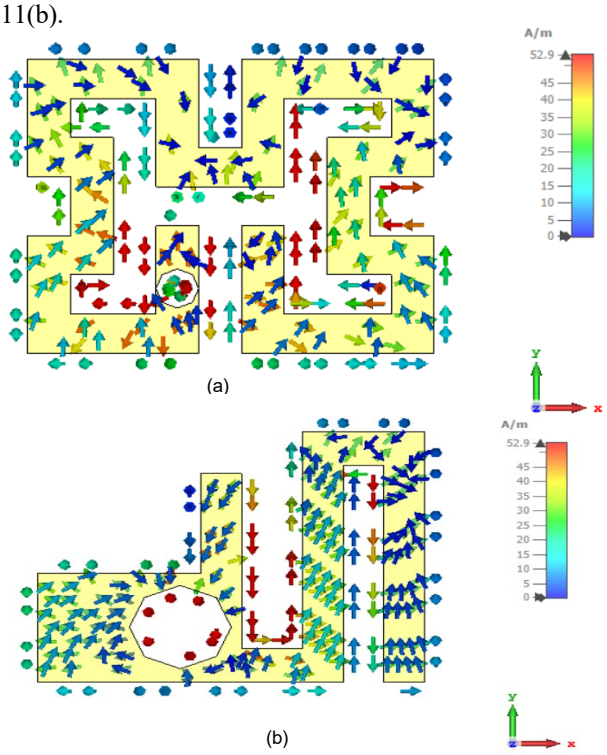

FIGURE 11. The current distribution across the surface of the antenna's (a) Patch, as observed within the 2.48 GHz (b) Ground

The obtained radiation pattern of the recommended antenna at a frequency of 2.45 GHz is shown in Fig. 12, which is the suggested model simulated inside the tissue of the human body. The antenna shows peak gains of −39.8 dBi at 2.48 GHz. The obtained radiation pattern of the recommended antenna at a frequency of 2.45 GHz is shown in Fig. 12, which is the suggested model simulated inside the tissue of the human body. The antenna shows peak realized gains of −41dBi at 2.48 GHz. The integration of a high-permittivity superstrate layer (e.g., Al_2O_3, $\varepsilon_r \approx 9$) is a key strategy to enhance gain. This approach concentrates electromagnetic fields near the antenna, reduces power dissipation in lossy tissues, and improves radiation directivity toward the skin surface.

B. SAR RESULTS

When implementing an ingestible wireless capsule endoscopy (WCE) system, assessing the specific absorption rate (SAR) represents an essential element in patient safety [19]. SAR can be evaluated as follows [20],[32]:

$$SAR = \frac{\sigma E^2}{2\rho} \tag{2}$$

E, σ, and ρ represent the tissues' electrical field magnitude, conductivity, and mass density, respectively. A 2 W/kg restricted averaged SAR value is aligned with the revised IEEE C95.1-2019 standard at the maximum of 10 g[21]-[22]. The human muscle phantom with the implanted capsule, as depicted in Fig. 3, is employed to assess the SAR evaluations. It is crucial to note that these specific absorption rate (SAR) analyses are executed with an input power of 1 watt supplied at the antenna port. The results expose that the simulated maximum 1-g average SAR value is 382 W/kg at 2.48 GHz. At the same time, the SAR value for the 10 g standard is 39.6 W/kg.

Consequently, the corresponding maximum input power level for frequency is calculated as the maximum allowable power needed to meet the protection standard of 1.6 W/kg for a specific absorption rate of 1 g, given a SAR of 382 W/kg, which is 4.2 milliwatts. These results confirm the safety and Suitability of the suggested antenna model for utilization within the human body. Fig. 13 illustrates the specific absorption rate SAR of the proposed Model.

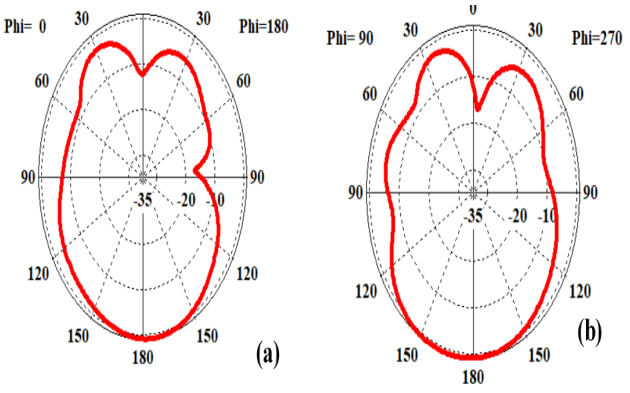

FIGURE 12. The simulated radiation patterns for the proposed antenna.

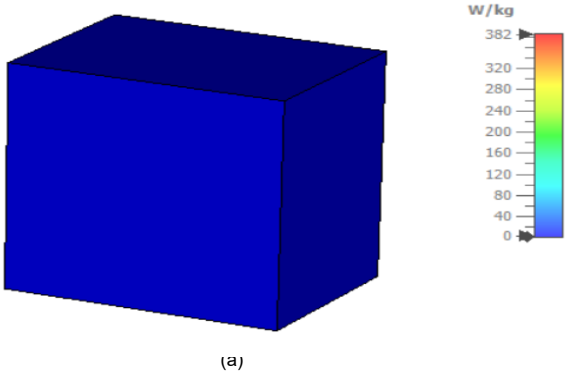

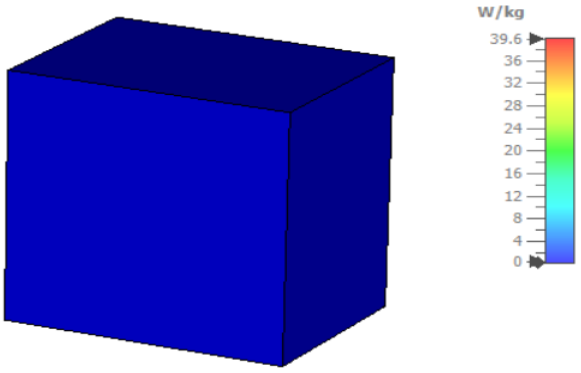

(b)

FIGURE 13. (a) Specific Absorption Rate (SAR) of 1 g of human tissue at a band of 2.45 GHz, (b) SAR of 10 g of tissue of the human body at a band of 2.45 GHz.

C. ANTENNA FABRICATION

Etching technology was used to fabricate the proposed configuration of the biomedical implantable MPA. The miniaturized size of 1.9 mm × 1.5 mm ×0.12 mm of the prototype antenna is manufactured on a Rogers RO3010 substrate having a dielectric constant ε_r=10.2 and loss tangent of tanδ 0.0022. Among the various antenna miniaturization techniques, utilizing high permittivity substrates is considered one of the most straightforward approaches. Then, an SMA coaxial cable is soldered to the fabricated antenna prototype for feeding without using a superstrate on the top of the antenna. Next, PC capsule endoscopy encapsulates the antenna and electronic components. Fig. 14 demonstrates the final configuration of the manufactured antenna prototype.

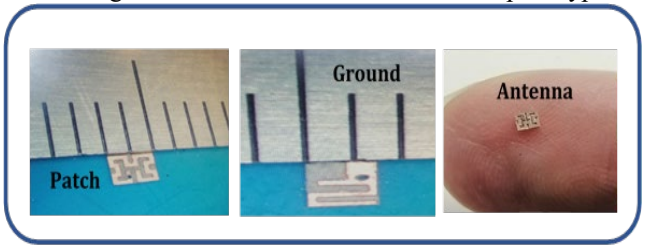

FIGURE 14. Fabricated microstrip patch implantable antenna.

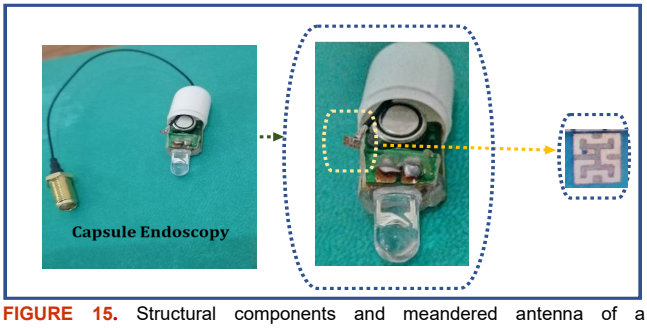

FIGURE 15. Structural components and meandered antenna of a miniaturized endoscopic capsule.

IV. EMPIRICAL ASSESSMENTS AND RESULTS

After the desired results are attained, and the antenna is carefully manufactured, then encapsulated within a biocompatible casing, as shown in Fig.15. This capsule engages a dummy component, tending to more reality, including batteries, an LED, and a PCB. An antenna's return loss (S_{11}) was tested with the capsule in a container filled with minced cow meat. The dimensions of this container were 80 mm × 90 mm × 60 mm, with a depth of implant of 50 mm. The experimental setup included placing the antenna in the middle of a container, as depicted in Fig.16, facilitating the minced beef cow handling easier.

Accentuating the novelty and advantages of the proposed investigation, a thorough comparative analysis has been conducted with previously documented endoscopy implantable antennas, as detailed in Table III.

Subsequently, the measured and simulated antenna reflection coefficient (S_{11}) at ISM frequency bands are compared. The experimental results confirm the applicability of the antenna with the resonances falling within the target ISM 2.4-2.48 GHz bands, as depicted in Fig. 17, indicating it is a good candidate for use in medically implanted devices MIDs given its capability to execute well within the human body environment. While this study presents comprehensive simulations of the proposed antenna's realized gain and radiation patterns, we acknowledge the absence of experimental measurements to validate these results. Based on previous studies and theoretical expectations, we anticipate that the measured realized gain will align closely with our simulated results. However, discrepancies may arise due to factors such as fabrication imperfections, environmental conditions, and measurement setup.

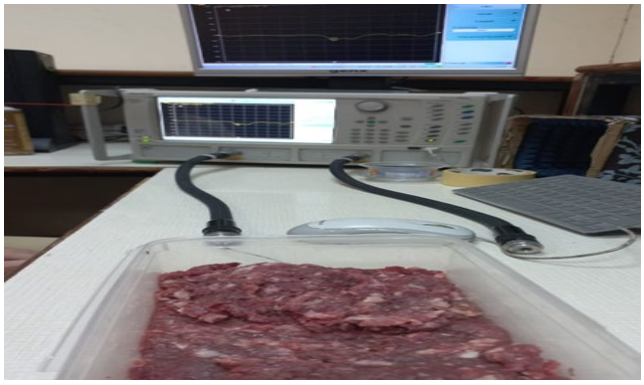

FIGURE 16. Experimental setup of the recommended antenna.

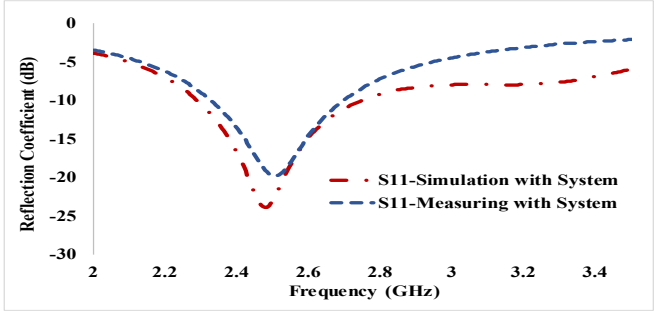

FIGURE 17. Measured and simulated the suggested microstrip antenna's reflection coefficient (S_{11}).

TABLE III. Comparative Evaluation of the Proposed Miniaturized Antenna Design Against Previously Reported Implantable Antennas for Endoscopic Applications.

Ref.	Freq GHz	Size	BW%	Gain /dBi	Depth of Imp. mm
[23]	UWB 6.6-9.6	0.32 λ × 0.213 λ × 0.0525 λ	37.04	-11.8	-
[24]	2.45	0.041 λ × 0.034 λ × 0.001 λ	25.2	−22.7	80
[27]	0.915 1.4 2.4	0.0107λ×0.0517λ×π	179.8	-24.6	50
[28]	2.45	0.0439λ×0.0508λ× 0.001λ	13	−20.5	75
[29]	0.920 2.45	0.0307 λ×0.0307 λ× 0.0018 λ	123	- 29.33 -20	2
[30]	1.4 2.45	0.0383 λ×0.0383 λ× 0.00297 λ	7.2 1.4	-29.4 -30.4	75
[20]	0.915 2.45	0.0198λ×0.0198λ× 0.00015 λ	13.63 6.28	−29.4	50
[31]	2.48	0.021λ₀ × 0.017λ₀ × 0.001λ₀	16.13%	−33	20
This work	2.45	0.0156 λ×0.0123 λ× 0.0010 λ	18.2	-39.8	50

V. CONCLUSION

This systematic work introduces an exceptionally miniaturized implantable antenna engineered to fulfill the distinct requirements of compact Implantable Medical Devices (IMDs) for the emerging field of capsule endoscopy applications. Featuring an extraordinarily compact footprint and a volume of merely 0.3 mm³, the antenna exhibits specific frequency operation, encompassing the Industrial, Scientific, and Medical at 2.48 MHz for capsule endoscopy. Furthermore, the safety of the antenna was evaluated by IEEE SAR regulations. The 1-g SAR value is 382 W/kg at 2.48 GHz. Additionally, different implementation scenarios were executed, including muscle, stomach, and small intestine, making it robust to the effects of implantation in various human body parts, owing to the result of bandwidth getting 483MHz. Finally, the antenna design exhibits promising potential as a suitable candidate for implantable medical devices in capsule endoscopy devices.

REFERENCES

[1] C. Xinkai, *et al*, A wireless capsule endoscopic system with a low-power controlling and processing ASIC. In *Proceedings of the 2008 IEEE Asian Solid-State Circuits Conference (A-SSCC)*, vol. 3, no. 1, pp. 321–324. DOI: 10.1109/ASSCC.2008.4708792. 2008

[2] M. Phillip, R. Harish, and R. Yahya, " Conformal ingestible capsule antenna: A novel chandelier meandered design,_" *IEEE Transactions on Antennas and Propagation*, 2009, vol. 57, no. 4 PART 1, pp. 900–909. DOI: 10.1109/TAP.2009.2014598.

[3] A. Psathas, K. Asimina, and S. Konstantina, "A novel conformal antenna for ingestible capsule endoscopy in the MedRadio Band," *In Proceedings of the Progress in Electromagnetics Research Symposium*. 2013, pp. 1899-1902.

[4] H. Saber, A. Hend, and A. Asmaa, "Octafilar helical antenna for circular polarization wireless capsule endoscopy applications, " *Wireless Personal Communications*, 2019, vol. 108, no. 1, pp. 569–579. DOI: 10.1007/s11277-019-06418-7.

[5] Y. Muhammad, *et al*. "Compacted conformal implantable antenna with multitasking capabilities for ingestible capsule endoscope, " *IEEE Access*, 2020, vol. 8, pp. 157617–157627. DOI: 10.1109/ACCESS.2020.3019663.

[6] A. Ala, " Compact wideband antenna for wireless capsule endoscopy system , " *Applied Physics A: Materials Science and Processing*, 2021, vol. 127, no. 4. DOI: 10.1007/s00339-021-04420-0.

[7] Z. Zhang, *et al*. "A conformal differentially fed antenna for ingestible capsule system," *IEEE Transactions on Antennas and Propagation*, 2018, vol. 66, no. 4, pp. 1695-1703. DOI: 10.1109/TAP.2018.2804673.

[8] J. Jong, W. Se, and T. Youn, "2.4 GHz wide-bandwidth inverted-F antenna for capsule endoscope," *Microwave and Optical Technology Letters*, 2020, vol. 62, no. 3, pp. 1275–1280. DOI: 10.1002/mop.32134.

[9] R. Md, *et al*. "In-body antenna for wireless capsule endoscopy at MICS band," *Advances in Intelligent Systems and Computing*, , vol. 857, pp. 801–810. DOI: 10.1007/978-3-030-01177-2_59. 2019.

[10] R. Rongqiang, X. Yong, and D. Guohong, "A conformal circularly polarized antenna for wireless capsule endoscope systems," *IEEE Transactions on Antennas and Propagation*, 2018, vol. 66, no. 4, pp. 2119–2124. DOI: 10.1109/TAP.2018.2804674.

[11] D. Rupam, and Y. Hyoungsuk, "A wideband circularly polarized conformal endoscopic antenna system for high-speed data transfer," *IEEE Transactions on Antennas and Propagation*, 2017, vol. 65, no. 6, pp. 2816–2826. DOI: 10.1109/TAP.2017.2694700.

[12] R. BANSAL, "Antenna theory; analysis and design," 2008, vol. 72, no. 7. DOI: 10.1109/proc.1984.12959.

[13] Z. Muhammad, A. Izaz, and Y. Hyoungsuk, "Metamaterial-loaded compact high-gain dual-band circularly polarized implantable antenna system for multiple biomedical applications," *IEEE Transactions on Antennas and Propagation*, 2020, vol. 68, no. 2, pp. 1140–1144. DOI: 10.1109/TAP.2019.2938573.

[14] A. Iqbal, A. Muath, B. Ismail, and A. Tayeb, "Self-quadruplexing antenna for scalp-implantable devices," IEEE *Transactions on Antennas and Propagation*, 2024, vol. 72, no. 3, pp. 2252–2260. DOI: 10.1109/TAP.2024.3356061.

[15] L. Abdenasser, E. Ahmed, G. Vicente, and S. Daniel "Miniaturized dual-band implantable antenna for implanted biomedical devices," *IEEE Access*, 2024, vol. 12, pp. 15026–15036. DOI: 10.1109/ACCESS.2024.3357488.

[16] D. Bradley, S. Salil, W. Yvonne, and G. Keat "Wireless technologies for implantable devices," *Sensors* (Switzerland), 2020, vol. 20, no. 16, pp. 1–19. DOI: 10.3390/s20164606.

[17] S. GABRIEL, R. LAU, and C. GABRIEL, "The dielectric properties of biological tissues: III. Parametric models for the dielectric spectrum of tissues. 1996. [Online]. Available: http://iopscience.iop.org/0031-9155/41/11/003.

[18] Z. Ahmed, *et al*. "Design and modeling of ultra-compact wideband implantable antenna for wireless ISM band," *Bioengineering*, 2023, vol. 10, no. 2. DOI: 10.3390/bioengineering10020216.

[19] L. Ben, W. Yifan, Z. Junchi, and S. Jingjing, "Ultra-wideband antennas for wireless capsule endoscope system: A review, " *IEEE Open Journal of Antennas and Propagation*, 2024, vol. 5, no. 2, pp. 241–255. DOI: 10.1109/OJAP.2024.3355217.

[20] S. Hayat, A. Syed, and Y. Hyoungsuk, "Miniaturized dual-band circularly polarized implantable antenna for capsule endoscopic system," *IEEE Transactions on Antennas and*

Propagation, 2021, vol. 69, no. 4, pp. 1885–1895. DOI: 10.1109/TAP.2020.3026881.

[21] H, William. H., *et al*. "Synopsis of IEEE Std C95.1TM-2019' IEEE Standard for Safety Levels with Respect to Human Exposure to Electric, Magnetic, and Electromagnetic Fields, 0 Hz to 300 GHz," *IEEE Access*, 2019, vol. 7, pp. 171346–171356. DOI: 10.1109/ACCESS.2019.2954823.

[22] G. Ziegelberger, *et al*. "Gaps in knowledge relevant to the 'guidelines for limiting exposure to time-varying electric and magnetic fields (1 Hz-100 kHz*)*," *Health Physics*, 2020, vol. 118, no. 5, pp. 533–542. DOI: 10.1097/HP.0000000000001261.

[23] K. Mutiara, S. Bambang, and S. Miftadi, "Design of microstrip antenna for wireless capsule endoscopy in wireless body area network," *In Proceedings of the 2017 IEEE Asia Pacific Conference on Wireless Mobile*. 2017, pp. 134–137. DOI: 10.1109/APWiMob.2017.8283996.

[24] J. Abdullah, and A. Amjad, "A compact and wideband MIMO antenna for high-data-rate biomedical ingestible capsules," *Scientific Reports*, 2022, vol. 12, no. 1. DOI: 10.1038/s41598-022-18468-2.

[25] E. Atashpanjeh, and P. REZAEI, "Broadband conformal monopole antenna loaded with meandered arms for wireless capsule endoscopy," *Wireless Personal Communications*, 2020, vol. 110, no. 4, pp. 1679–1691. DOI: 10.1007/s11277-019-06806-z.

[26] H. Syed, I. Ali, and Y. Hyoungsuk, "Ultra-miniaturized implantable antenna enabling multiband operation for diverse industrial IoMT devices," *IEEE Transactions on Antennas and Propagation*, 2024, vol. 72, no. 2, pp. 1352–1362. DOI: 10.1109/TAP.2024.3349782.

[27] N. Rakesh, *et al*. "Design and validation of loop-based ultraminiature low-profile ultrawideband capsule antenna inside Wistar rat." *IEEE Transactions on Antennas and Propagation*, vol. 71, no. 10, pp. 8326–8331, 2023.DOI: 10.1109/TAP.2023.3301952,

[28] J. Abdullah, and I. Amjad, "A high data rate implantable MIMO antenna for deep implanted biomedical devices," *IEEE Transactions on Antennas and Propagation*, 2022, vol. 70, no. 2, pp. 998–1007. DOI: 10.1109/TAP.2021.3111186.

[29] S. Gopinath, and D. Debasis, "Dual-band circular polarized flexible implantable antenna using reactive impedance substrate," *IEEE Transactions on Antennas and Propagation*, 2019, vol. 67, no. 6, pp. 4218–4223. DOI: 10.1109/TAP.2019.2905978.

[30] A. Abdullah, *et al*. "Ultraminiaturized dual-band implantable antenna for wireless capsule endoscopy,". *IEEE Sensors Journal,* vol. 24, no. 9, pp. 15210–15218. 2024.

[31] M. M. Hassooni, J. S. Aziz, and A. Q. Hameed, "Design of an Ultra-Miniaturized Meandered Patch Antenna for Scalp Applications," Prog. Electromagn. Res. C, vol. 158, no. June, pp. 205–213, 2025, doi: 10.2528/PIERC25060219.

[32] M. M. Hassooni, J. S. Aziz, and A. Q. Hameed, "Ultra-Miniaturized Spiral Antenna for Loop Recorder," vol. 132, no. November 2024, pp. 21–30, 2025, doi: 10.2528/PIERM24112101.